Bioorganic & Medicinal Chemistry 17 (2009) 2536–2543

Contents lists available at ScienceDirect

Bioorganic & Medicinal Chemistry

journal homepage: www.elsevier.com/locate/bmc

The effect of linker length on binding affinity of a photoswitchable molecular glue for DNA

Chikara Dohno, Shin-nosuke Uno, Shun Sakai, Mika Oku, Kazuhiko Nakatani *

Department of Regulatory Bioorganic Chemistry, The Institute of Scientific and Industrial Research (SANKEN), Osaka University, 8-1 Mihogaoka, Ibaraki 567-0047, Japan

ARTICLE INFO

Article history:
Received 20 December 2008
Revised 21 January 2009
Accepted 22 January 2009
Available online 30 January 2009

Keywords:
DNA
Hybridization
Mismatch binding ligand
Photoswitchable molecular glue

ABSTRACT

Molecular glue for DNA is a small synthetic ligand that adheres two single-stranded DNAs to produce a double-stranded DNA. We previously devised a photoswitchable molecular glue (PMG) that uses external light stimuli to reversibly control DNA hybridization. To optimize the structure of PMG, we synthesized a series of PMGs and evaluated the effect of changing the methylene linker length on the binding affinity and photoresponse. From the comprehensive T_m and CSI-TOF-MS measurements, a PMG possessing a three-methylene linker with carbamate linkage produced maximum binding affinity and photoswitching ability. These results indicate that a small difference in the linker can significantly affect PMG function. These findings are useful for designing new photoswitchable DNA-binding ligands.

1. Introduction

The sequence-specific hybridization property of DNA is the unique and indispensable basis of the essential functions of DNA. Being able to control DNA hybridization with external stimuli could be useful for regulating diverse biological functions and constructing DNA-based materials. A wide variety of chemically modified oligonucleotides have been developed to control and modulate DNA hybridization.[1–7] We demonstrated previously a new concept of a molecular glue for DNA that controls the hybridization of two natural unmodified DNAs.[8] This molecular glue is a small synthetic ligand that adheres two single-stranded DNAs (ssDNA) that do not hybridize spontaneously with each other. We have developed a series of synthetic small molecules that can bind specifically to mismatch-containing DNAs.[8,9] Because the mismatch-binding ligands (MBLs) increase the apparent thermodynamic stability of the mismatched DNA duplex, MBLs can function as a molecular glue for DNA. The function of the molecular glue in the first generation was limited to the unidirectional control of DNA hybridization because MBL induces the one-way transformation from ssDNA to double-stranded DNA (dsDNA).[8] We previously extended the concept to the reversible control of DNA hybridization by external stimuli.[10] To accomplish this objective, we have devised a photoswitchable molecular glue (PMG) for DNA, **NCDA**, in which a photochromic azobenzene unit is incorporated into the GG mismatch-binding ligand. **NCDA** permits the reversible control between ssDNA and dsDNA containing a GG-mismatch by external light stimuli (Fig. 1).

The photochromic azobenzene moiety in **NCDA** exhibits *Z*/*E* isomerization in response to the light stimuli, which changes the relative position and orientation of the two naphthyridines. ***Z*-NCDA** can bind to DNA more strongly than can ***E*-NCDA** and, therefore, is more efficient as a molecular glue. The photoswitching ability is based on the difference of the stabilization effect between ***Z*-NCDA** and ***E*-NCDA**. To achieve an ideal switching of DNA hybridization, an increased binding affinity of ***Z*-NCDA** and a decreased binding affinity of ***E*-NCDA**, or vice versa, are desirable. To understand the structure–binding relationship of PMG, we herein describe our synthesis of a series of PMGs that possess common mismatch recognition groups and photochromic azobenzene but different linking groups (Chart 1). Investigation of the PMG function revealed a significant correlation between the linker structures and PMG function.

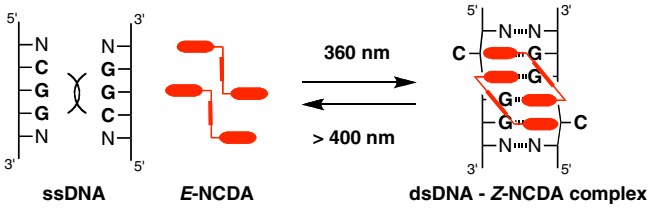

Figure 1. Control of DNA hybridization by photoswitchable molecular glue for DNA.

* Corresponding author. Fax: +81 6 6879 8459.
E-mail address: nakatani@sanken.osaka-u.ac.jp (K. Nakatani).

0968-0896/$ - see front matter © 2009 Elsevier Ltd. All rights reserved.
doi:10.1016/j.bmc.2009.01.053

2. Results and discussion

The parent PMG, **NCDA**, is constituted of base-recognizing naphthyridine moieties, a photochromic azobenzene, and a flexible linker connecting the two naphthyridines. The dimeric naphthyridine carbamate functions to recognize GG-mismatch DNA by forming complementary hydrogen bonds.[8,9c] The azobenzene moiety undergoes *Z*/*E* isomerization upon photoirradiation, and this photoisomerization induces changes in the DNA-binding affinity and stabilization ability of **NCDA**.[11] The photoinduced structural change of the azobenzene moiety is transmitted as a geometry change of the two naphthyridines through the linker. Therefore, the photoswitching ability of **NCDA** will be highly dependent on the linker group. From the standpoint of the large change in geometry, a short and rigid linker is favorable for maximum photoswitching ability of **NCDA**. However, a long and flexible linker is required to locate the two naphthyridines in the proper geometry, whereas a shorter linker is preferred to minimize the entropic costs. Thus, optimization of the linker length is required to maximize the switching ability of PMG.

To evaluate the effect on the switching property and binding affinity of PMG possessing different linkers, we synthesized a series of **NCDA** variants with methylene linker lengths ranging from two to four (Chart 1). **NCDA** with a four-methylene linker (**NCDA4**) was synthesized as shown in Scheme 1. 4-Aminobutanol **5** was converted to the four-methylene-linked naphthyridine derivatives **9b** via coupling its activated carbonic acid ester with 2-amino-7-methyl-1,8-naphthyridine. Reductive amination of the naphthyridine carbamate **9b** with 4,4′-diformyl-azobenzene furnished the desired **NCDA4** in moderate yield. Synthesis of **NCDA2** and **NCDA3**[10] was achieved via a similar reductive amination reaction in Scheme 1. However, it was difficult to isolate **NCDA2** in acceptable purity because of its instability. Decomposition with concomitant generation of **14**, **12**, and **13** suggested that **NCDA2** underwent a facile intramolecular carbamate exchange reaction, which is favored by the formation of a five-membered ring (Chart 2).[12] To overcome this difficulty, we developed another synthetic route where the final step is *N*-Boc deprotection of **21** (Scheme 2). In this synthetic scheme, **NCDA2** was obtained as a hydrochloric salt. The hydrochloric salt of **NCDA2** is chemically more stable because the protonation of the amines in **NCDA2** hinders the intramolecular carbamate exchange reaction by decreasing the nucleophilicity. **NDA** is an **NCDA** analogue possessing amide linkages instead of carbamate linkages (Scheme 1). The linker length is equivalent to one methylene linker in the **NCDA** series. All PMGs synthesized here have a poor solubility in water and were therefore used as hydrochloric salts in following experiments.

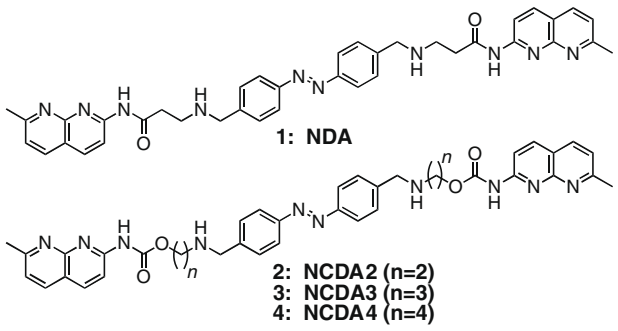

Chart 1.

Azobenzene is a well-known photochromic molecule that shows *E* to *Z* isomerization by UV light irradiation and *Z* to *E* isomerization by visible light irradiation.[12] Photoisomerization of **NCDA4** in aqueous 10 mM Na·cacodylate buffer (pH 7.0) and 100 mM NaCl was monitored by UV–vis absorption spectroscopy (Fig. 2). The spectrum before photoirradiation exhibited an absorption band at around 317 nm attributed to the overlap of the azobenzene π–π^* transition and absorption of naphthyridine chromophores. Upon exposure to 360 nm light, the band intensity at 317 nm decreased and the absorbance at around 405 nm increased concomitantly. These spectral changes are typical of the *E* to *Z* photoisomerization of azobenzene.[13] The photoisomerization of **NCDA4** was confirmed further by HPLC analysis. The azobenzene of **NCDA4** exists exclusively in the *E* form under ambient light condition (Fig. 3a). We examined the *E* to *Z* photoisomerization of **NCDA4** using UV light in 10 nm intervals at wavelengths ranging from 330 to 380 nm. The maximum *Z* isomer content in the photostationary states was achieved by 360 nm irradiation. After 5 min irradiation at 360 nm, the photostationary state was reached, and the fraction of *Z*-**NCDA4** increased to about 55% (Fig. 3b). The photostationary mixture was then irradiated with 430 nm light, resulting in conversion back to the mixture comprising exclusively *E*-**NCDA4** (Fig. 3c). Similar photoisomerization behaviors were observed for **NCDA2** and **NCDA3**, whereas **NDA** showed considerably higher *E* to *Z* photoisomerization efficiency (81% *Z* in the photostationary state).

We next examined the stabilization of mismatch DNA duplex by the series of **NCDA** derivatives and **NDA**. The melting temperatures

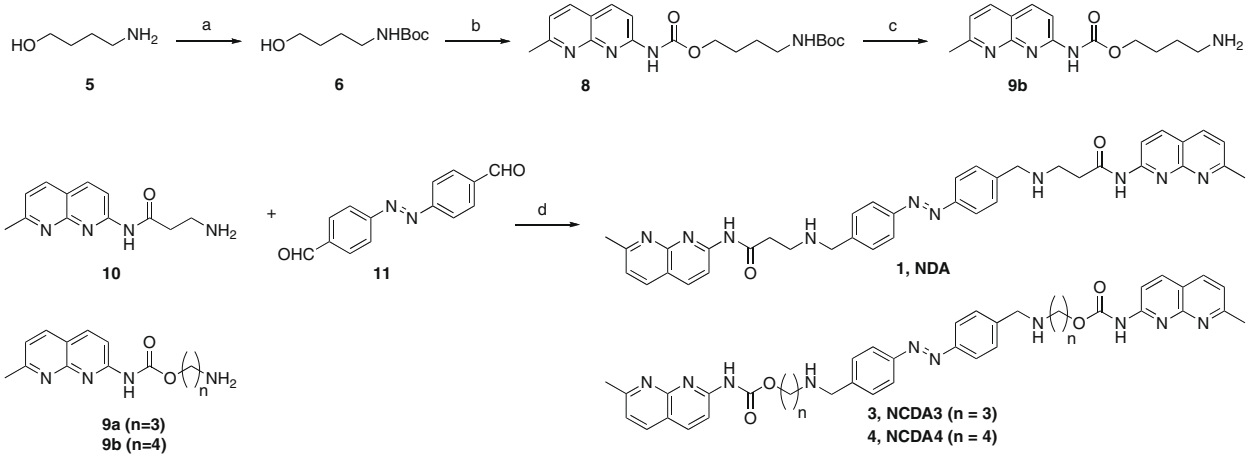

Scheme 1. Reagents and conditions: (a) Boc_2O, $CHCl_3$, quant.; (b) (i) DSC, Et_3N, CH_3CN; (ii) 2-amino-7-methyl-1,8-naphthyridine, Et_3N, CH_2Cl_2, 61% (two steps); (c) HCl, AcOEt, $CHCl_3$, 80%; (d-i) **10**, $NaBH_3CN$, AcOH, MeOH, $CHCl_3$, 14%; (d-ii) **9a**, $NaBH_3CN$, AcOH, MeOH, $CHCl_3$, 37%; (d-iii) **9b**, $NaBH_3CN$, AcOH, MeOH, $CHCl_3$, 50%.

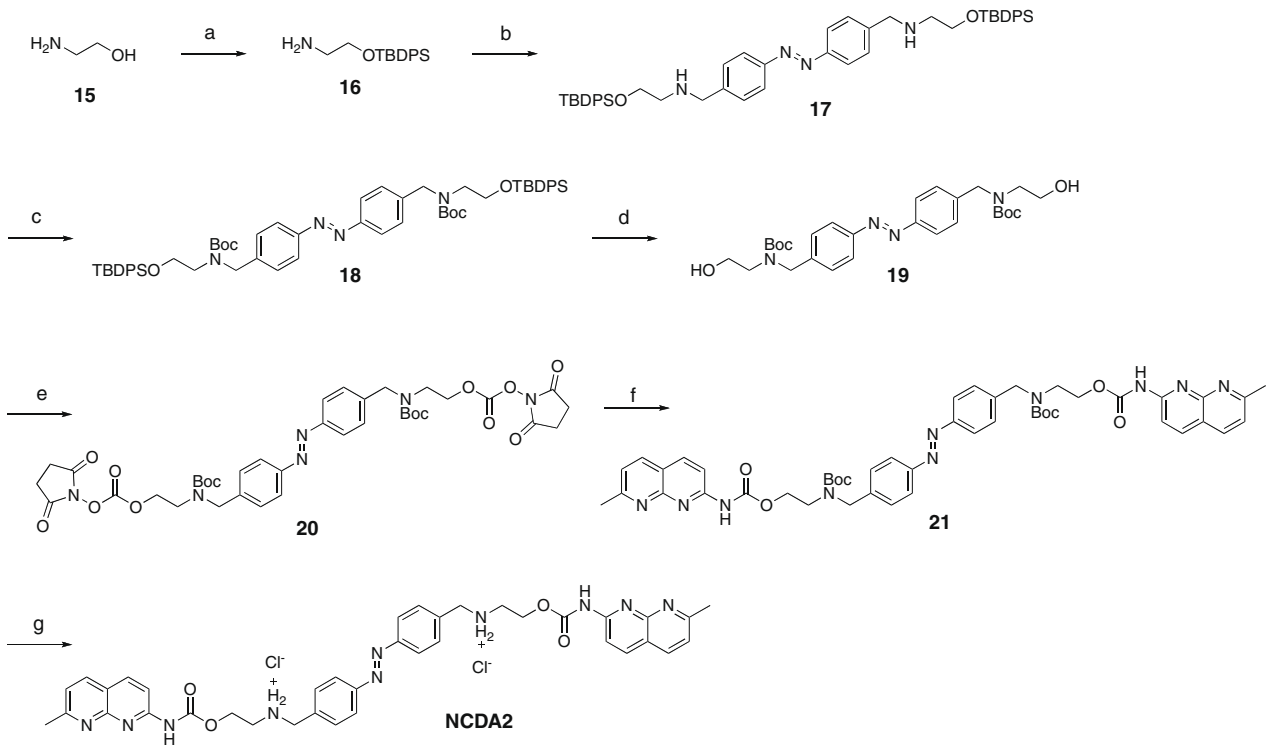

Scheme 2. Reagents and conditions: (a) TBDPSCl, imidazole, 43%; (b) 4,4′-diformylazobenzene **11**, $NaBH_3CN$, AcOH, CH_3OH, $CHCl_3$, 45%; (c) Boc_2O, $CHCl_3$, 84%; (d) TBAF, AcOH, THF, 93%; (e) DSC, Et_3N, CH_3CN, 67%; (f) 2-amino-7-methyl-1,8-naphthyridine, Et_3N, CH_2Cl_2, 56%. (g) HCl, AcOEt, $CHCl_3$, quant.

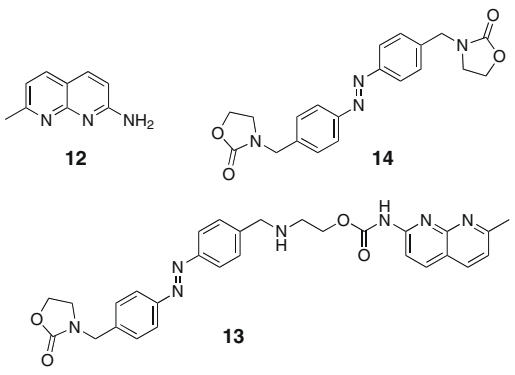

Chart 2.

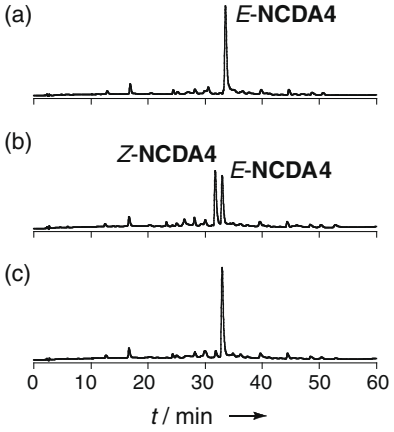

Figure 3. HPLC analysis of the photoisomerization of **NCDA4**. The solution of **NCDA4** (40 μM) in 10 mM Na·cacodylate (pH 7.0) and 100 mM NaCl was photoirradiated, and analyzed by HPLC. The peak with a longer retention time is attributed to *E*-**NCDA4**. Key: (a) Before irradiation; (b) after 360 nm irradiation for 5 min, (c) subsequent irradiation at 430 nm for 5 min.

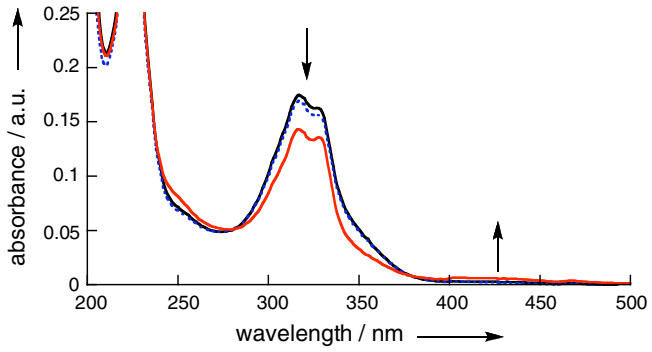

Figure 2. UV–vis spectra of **NCDA4** (6 μM) in 10 mM Na·cacodylate (pH 7.0) and 100 mM NaCl (black line). The sample was irradiated with 360 nm light for 10 min (red solid line). Subsequent irradiation at 430 nm for 5 min resulted in a recovery of the original spectrum (blue dotted line).

(T_m) of 11-mer duplexes 5′-(CTAA ***CXG*** AATG)-3′/5′-(CATT ***CYG*** TTAG)-3′ containing a single mismatch site (***X***/***Y***) were measured in the presence of the PMGs before and after photoisomerization (Table 1). All synthesized photoswitchable ligands have two guanine-recognizing naphthyridine groups, and, as expected, showed an apparent selectivity for duplexes containing a GG mismatch. Regardless of the linker length, the T_m values of the GG-mismatch duplex were higher after photoirradiation at 360 nm (T_{m2}) than before irradiation (T_{m1}), showing that PMGs in the *Z* configuration have a higher stabilization ability than the *E* isomer. This is probably because, for inducing the appropriate spatial arrangements of the two naphthyridine groups, the folded *Z* azobenzene linkage

Table 1
Melting temperature (T_m/°C) of DNA duplexes in the presence of a variety of PMGs before and after photoirradiation

X–Y	T_{m0}[a]	+**NCDA2**, dark		+**NCDA2**, *hν*		+**NCDA3**, dark		+**NCDA3**, *hν*	
		T_{m1}[b]	ΔT_{m1}[c]	T_{m2}[d]	ΔT_{m2}[e]	T_{m1}[b]	ΔT_{m1}[c]	T_{m2}[d]	ΔT_{m2}[e]
G–G	**25.6**	**28.9**	**3.4**	**42.7**	**13.8**	**32.7**	**7.1**	**48.0**	**15.2**
A–A	17.8	17.6	−0.2	17.9	0.3	n.d.[f]	n.d[f]	21.3	n.d.[f]
A–C	16.1	18.5	2.4	19.4	0.9	23.3	7.2	20.4	−2.9
C–C	18.2	24.5	6.3	24.6	0.1	25.7	7.4	22.7	−3.0
G–A	25.7	27.1	1.4	31.6	4.5	32.0	6.3	33.4	1.4
G–T	28.3	30.9	2.6	32.6	1.7	32.0	3.7	31.5	−0.5
T–C	18.6	21.1	2.5	21.2	0.1	27.2	8.6	23.8	−3.4
T–T	25.1	22.3	−2.8	24.1	1.8	28.6	3.5	27.8	−0.8
A–T	34.3	33.7	−0.6	33.5	−0.2	34.5	−0.2	35.2	0.7
G–C	40.3	40.8	0.5	40.9	0.1	38.6	−1.7	40.3	1.7

X–Y	+**NCDA4**, dark		+**NCDA4**, *hν*		+**NDA**, dark		+**NDA**, *hν*	
	T_{m1}[b]	ΔT_{m1}[c]	T_{m2}[d]	ΔT_{m2}[e]	T_{m1}[b]	ΔT_{m1}[c]	T_{m2}[d]	ΔT_{m2}[e]
G–G	**30.3**	**4.7**	**38.3**	**8.0**	**37.3**	**11.7**	**38.6**	**1.3**
A–A	n.d.[f]	n.d.[f]	n.d.[f]	n.d.[f]	20.8	2.9	21.0	0.2
A–C	n.d.[f]	n.d.[f]	n.d.[f]	n.d.[f]	18.3	2.2	17.9	−0.4
C–C	25.8	7.6	25.3	−0.5	23.1	4.9	22.5	−0.6
G–A	26.0	0.3	25.4	−0.6	30.0	4.3	30.1	0.1
G–T	30.0	1.7	30.3	0.2	24.2	−4.1	25.4	1.2
T–C	24.4	5.8	24.0	−0.4	22.0	3.4	22.2	0.2
T–T	28.3	3.2	27.1	−1.2	n.d.[f]	n.d.[f]	n.d.[f]	n.d.[f]
A–T	36.2	1.9	36.1	−0.1	31.8	−2.5	30.2	−1.5
G–C	41.7	1.4	41.7	0.0	40.1	−0.2	40.2	0.1

The synthetic ligands were designed to bind selectively to GG-mismatch DNA, and the values for GG-mismatch were emphasized by the bold characters.

[a] T_m values of DNA duplexes in the absence of PMG. Thermal melting curves were measured for duplex DNA, d(CTA ACX GAA TG)/d(CAT TCY GTT AG) (4.54 μM) in 10 mM sodium cacodylate buffer (pH 7.0) containing 0.1 M NaCl. T_m values (°C) were calculated by median method.

[b] T_m values in the presence of PMG (18.2 μM).

[c] ΔT_{m1} is calculated as the difference between T_{m0} and T_{m1}.

[d] T_m values in the presence of PMG after photoirradiation at 360 nm for 5 min.

[e] ΔT_{m2} is calculated as the difference between T_{m1} and T_{m2}.

[f] T_m value could not be determined due to the unclear transition.

gives preferable binding compared with the extended *E* azobenzene linkage.[10] The binding of the *E* isomer is less selective to the GG mismatch than the binding of the *Z* isomer. The intercalative interaction of the planar *E* azobenzene may contribute to this less selective binding.[14]

The ΔT_{m2} value was calculated as the difference in T_m from before to after photoirradiation, and was used as an index of the photoswitchable function of the molecular glues. Among the four ligands tested, **NCDA3** possessing the three-methylene linker exhibited the highest ΔT_{m2} value (15.2 °C). Both the longer linker (**NCDA4**) and the shorter linkers (**NDA**, **NCDA2**) reduced the binding affinity and produced a less effective photoswitchable molecular glue. An ideal photoswitchable molecular glue will bind strongly in the *Z* configuration (high T_{m2} value) while keeping the affinity weak in the *E* configuration (low T_{m1} value). ***Z*-NCDA3** provides a significantly higher binding affinity to the GG-mismatch DNA (T_{m2} = 48.0 °C) than the other ligands, and this can overwhelm the relatively strong affinity of ***E*-NCDA3** (ΔT_{m1} = 7.1 °C). A single methylene unit insertion significantly decreased the T_{m2} value by 9.7 °C and ΔT_{m2} value by 7.2 °C (T_{m2} = 38.3 °C and ΔT_{m2} = 8.0 °C for **NCDA4**). **NCDA2** showed a photoresponse (ΔT_{m2} = 13.8 °C) comparable to **NCDA3**, but further shortening of the linker abolished the photoswitching ability (ΔT_{m2} = 1.3 °C for **NDA**). The exceptionally small T_m difference for **NDA** before and after photoirradiation is attributed to the considerably strong binding of ***E*-NDA** to GG-mismatch DNA (ΔT_{m1} = 11.7 °C). The effective binding of ***E*-NDA** raises the possibility of rational design of a new PMG possessing an opposite photoresponse, that is, higher binding affinity in the *E* configuration than in the *Z* configuration. The T_m data for **NDA** differed markedly from the **NCDA** series, suggesting a different binding mode. The maximum photoresponse was observed for **NCDA3** possessing three methylene units. These results clearly demonstrate that the linker structure and length affect the photoresponse significantly.

To examine the binding stoichiometry of PMGs, cold-spray ionization time-of-flight mass spectrometry (CSI-TOF-MS)[15] was used to measure the ligand–DNA complex before and after photoirradiation. The 11-mer duplex DNA 5′-(CTAA ***CGG*** AATG)-3′/5′-(CATT ***CGG*** TTAG)-3′ was used in these experiments because we previously found that dimeric naphthyridine derivatives bind selectively to the CGG/CGG sites with 2:1 stoichiometry or two ligands for a single CGG–CGG site (Fig. 1).[8,9] In the presence of 3 equiv of ***E*-NCDA** derivatives, the 5^- ions of the 1:1 complex (*m/z* of 1481.29, 1487.05, and 1492.54 for **NCDA2**, **NCDA3**, and **NCDA4**, respectively) and, to a lesser extent, the 2:1 complex (*m/z* of 1621.17, 1632.55, and 1643.43 for **NCDA2**, **NCDA3**, and **NCDA4**, respectively) were observed (Fig. 4a–d). After photoirradiation at 360 nm for 5 min, the ion intensity corresponding to the 2:1 complex increased markedly for all tested ligands (Fig. 4e–h); in particular, ***Z*-NCDA3** produced the 2:1 complex almost exclusively (Fig. 4f). The higher ion intensities compared with those before irradiation suggest that the ***Z*-NCDA** derivatives formed a more stable complex with the CGG–CGG sequence than did the ***E*-NCDA**, and these results agreed with the results of the T_m experiments. With increasing amounts of **NCDA** from 1 to 3 equiv, the ions corresponding to the 2:1 complex increased, but complexes with higher binding stoichiometries could not be detected under these conditions. The preferential formation of the 2:1 complex is typical

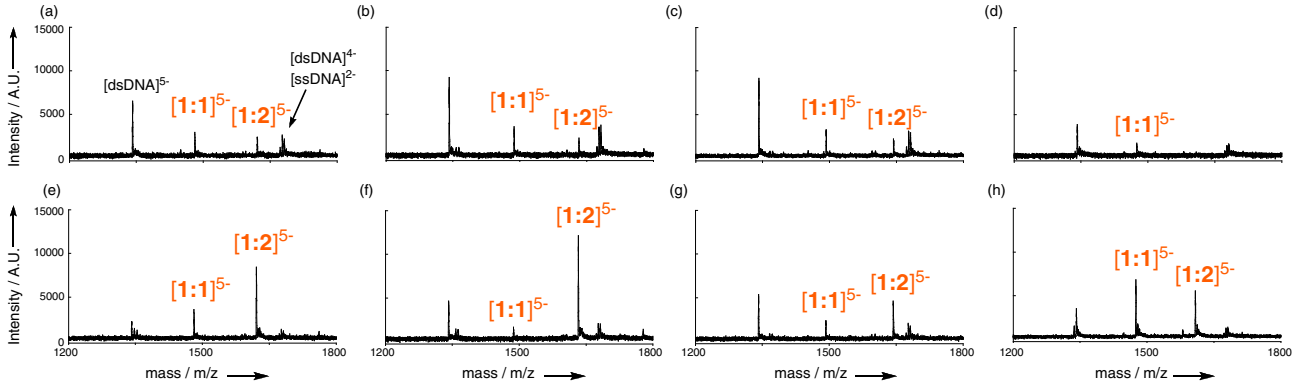

Figure 4. Cold-spray ionization time-of-flight mass spectra of DNA duplex in the presence of various PMGs. Samples contain 20 μM duplex DNA and 60 μM PMG in 50% aqueous methanol and ammonium acetate (100 mM). The sample was cooled at −10 °C during the injection with a flow rate 10 μL/min^{-1}. Key: (a)–(d) Before photoirradiation; (e)–(h) after photoirradiation at 360 nm for 5 min; (a) and (e) **NCDA2**; (b) and (f) **NCDA3**; (c) and (g) **NCDA4**; (d) and (h) **NDA**.

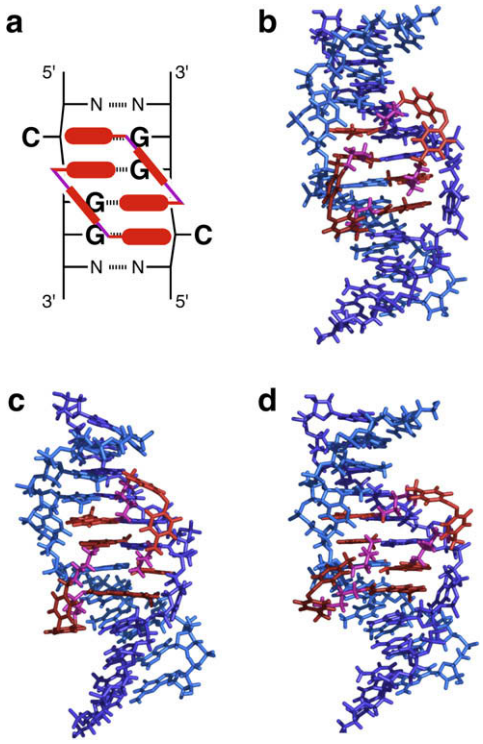

Figure 5. Molecular modeling of the complex between **NCDA** derivatives and the duplex DNA 5′-(CTAA ***CGG*** AATG)-3′/5′-(CATT ***CGG*** TTAG)-3′. The model structures were optimized by use of the AMBER* force field in water with MacroModel Version9.1. (a) Schematic illustration of the complex. (b) **NCDA2**; (c) **NCDA3**; (d) **NCDA4**. The ligands are represented in red, while their linker groups are represented in magenta.

for MBLs we have synthesized previously.[8–10] Figure 5 shows the predicted structure of the 2:1 complex of the *Z*-**NCDA** derivatives and the CGG/CGG containing 11-mer duplex DNA. These structures were obtained by energy minimization of the model structures constructed manually from the NMR-structure we previously determined[9b] using MacroModel 9.1 with an AMBER* force field in water. As increasing the linker length, the azobenzene moieties were more extruded from the major groove. Solvent accessible surfaces of the **NCDA** derivatives in the complex are calculated as 648, 665, and 772 Å^2 for **NCDA2**, **NCDA3**, and **NCDA4**, respectively, in the energy minimized structures. The hydrophobic azobenzene and the linking methylene groups of **NCDA4** in the complex are more exposed to solvent water (Fig. 5d). Thus, the long flexible methylene linker of **NCDA4** is unfavorable with regard to entropic costs that originate from the loss of degrees of freedom and the exposure of the hydrophobic groups to solvent water. The structure of the complex with **NCDA2** and **NCDA3** are similar in terms of the solvent accessible surfaces. The modestly weak binding of **NCDA2** may come from the existence of the remarkably stable conformations of the free ligand, which were obtained from conformational search calculations. The conformational change of the ligands upon the complex formation was estimated from the difference between the global minimum conformation of the free ligand and the conformation extracted from the ligand in the minimized structure of the complex. The conformational change of **NCDA2** in the complex formation was energetically less favorable than that of the **NCDA3** by 6.4 kJ/mol.

In contrast to the preferential formation of the 2:1 complex by **NCDA** derivatives, **NDA** prefers to form a 1:1 complex even in the *Z* configuration (Fig. 4h). The binding mode of **NDA** differs from that of the **NCDA** derivatives, probably because the linker is too short to form the above-mentioned 2:1 complex. The different binding mode may have caused the distinct binding properties observed in the T_m experiments (Table 1). The linker length is one methylene unit shorter in **NDA** than in **NCDA2** and has an amide linkage instead of a carbamate linkage. These changes in the linker have a significant effect on the DNA binding and the photoswitching properties. The optimal linker length is determined by a delicate balance of the enthalpic gain and the entropic loss upon ligand binding.

3. Conclusion

We synthesized and examined a series of the photoswitchable DNA-binding ligands to evaluate the effect of the differing methylene linker length on the binding affinity and photoresponse. This study reveals that the linker length has a significant effect on the binding affinity and the photoswitching ability. Therefore, determination of an optimal linker, which locates the base-recognizing moiety in the appropriate positions and minimize steric hindrance and entropic loss upon binding to the target DNA, is a crucial step. From the comprehensive T_m and CSI-TOF-MS measurements, both maximum binding affinity and photoswitching ability were observed for the three-methylene linker with carbamate linkage, **NCTA3**. The significantly higher binding affinity of *Z*-**NCDA3** than *E*-**NCDA3** contributes the remarkable photoresponse. A difference of only one methylene unit in the linker length has a profound influence on PMG function. In the case of **NDA** in particular, the two-methylene linker with amide linkage diminished the effective photoswitching. These findings provide useful guidance for designing new PMGs possessing different binding selectivity and photoresponse.

4. Experimental

4.1. General

Reagents and solvents were purchased from standard suppliers and used without further purification. Reactions were monitored with TLC plates precoated with Merck Silica Gel 60 F_{254}. Spots were visualized with UV light or ninhydrin. Wakogel C-200 was used for silica gel flash chromatography. ^{1}H NMR spectra were measured with JEOL JNM-LA400 and LA600. The chemical shifts are expressed in ppm relative to residual solvent as an internal standard. ESI mass spectra were recorded on a JEOL AccuTOF JMS-T100N mass spectrometer. FAB mass spectra were recorded on a JEOL JMS-M600H.

4.1.1. *N*-(7-Methyl-1,8-naphthyridin-2-yl)carbamic acid 4-(*tert*-butoxycarbonylamino)butyl ester (8)

To a mixture of *N*-(*tert*-butoxycarbonyl)-4-amino-1-butanol **6** (2.00 g, 10.7 mmol) and *N*,*N*-disuccinimidyl carbonate (DSC) (4.06 g, 15.9 mmol) in acetonitrile (30 mL) was added triethylamine (4.42 mL, 31.7 mmol) and the reaction mixture was stirred at ambient temperature for 3 h. Solvent was removed in vacuo and the residue was diluted with saturated aqueous $NaHCO_3$ solution and extracted with ethyl acetate. The organic phase was washed with brine, dried over anhydrous $MgSO_4$, filtered, and concentrated in vacuo. The crude product was purified by column chromatography on silica gel ($CHCl_3$/methanol = 100:1) to give crude succinimidyl carbonic ester **7** (3.36 g). To a solution of **7** (2.00 g, 6.05 mmol) in anhydrous dichloromethane (50 mL) was successively added 2-amino-7-methyl-1,8-naphthyridine (1.06 g, 6.66 mmol) and triethylamine (1.27 mL, 9.08 mmol) and the reaction mixture was stirred overnight at ambient temperature. The reaction mixture was diluted with saturated aqueous $NaHCO_3$

solution and extracted with $CHCl_3$. The organic phase was washed with brine, dried over anhydrous $MgSO_4$, filtered, and concentrated in vacuo. The crude product was purified by column chromatography on silica gel (ethyl acetate/*n*-hexane = 1:1) to give **8** (1.44 g, 3.85 mmol, 61% 2 steps from **6**) as a pale yellow solid: ^{1}H NMR (400 MHz, $CDCl_3$) δ = 1.42 (s, 9H), 1.59 (m, 2H), 1.74 (m, 2H), 2.75 (s, 3H), 3.16 (m, 2H), 4.22 (t, 2H, *J* = 6.6 Hz), 4.55 (br, 1H), 7.26 (d, 1H, *J* = 8.3 Hz), 7.72 (br, 1H), 7.99 (d, 1H, *J* = 8.3 Hz), 8.11 (d, 1H, *J* = 8.8 Hz), 8.25 (d, 1H, *J* = 8.8 Hz); ^{13}C NMR (150 MHz, $CDCl_3$) δ = 25.44, 25.98, 26.41, 28.26, 39.96, 65.25, 79.00, 112.49, 117.79, 121.14, 136.23, 138.81, 153.11, 153.31, 154.53, 155.85, 163.00; ESI-MS, *m/e* 397 ([M+Na]$^+$); HRMS (FAB): calcd for $C_{19}H_{27}O_4N_4$ ([M+H]$^+$) 375.2032, found 375.2042.

4.1.2. *N*-(7-Methyl-1,8-naphthyridin-2-yl)carbamic acid 4-aminobutyl ester (9b)

To a solution of **8** (500 mg, 1.34 mmol) in $CHCl_3$ (10 mL) was added ethyl acetate (1.67 mL) containing 4 M HCl and the reaction mixture was stirred at ambient temperature for 1 h. To the reaction mixture was added additional ethyl acetate containing 4 M HCl (1.00 mL). After 30 min stirring, solvent was removed in vacuo and the residue was washed with $CHCl_3$, diluted with saturated aqueous $NaHCO_3$ solution and extracted with $CHCl_3$. The organic phase was washed with brine, dried over anhydrous $MgSO_4$, filtered, and concentrated in vacuo to give **9b** (292 mg, 1.07 mmol, 80%) as a pale yellow solid: ^{1}H NMR (400 MHz, $CDCl_3$) δ = 1.52 (m, 2H), 1.72 (m, 2H), 2.69 (s, 3H), 2.72 (t, 2H, *J* = 7.1 Hz), 4.18 (t, 2H, *J* = 6.6 Hz), 7.20 (d, 1H, *J* = 8.0 Hz), 7.93 (d, 1H, *J* = 8.0 Hz), 8.05 (d, 1H, *J* = 8.8 Hz), 8.19 (d, 1H, *J* = 8.8 Hz); ^{13}C NMR (150 MHz, $CDCl_3$) δ = 25.59, 26.22, 29.69, 41.62, 65.66, 112.67, 117.94, 121.28, 136.40, 138.91, 153.32, 153.50, 154.69, 163.15; ESI-MS, *m/e* 297 ([M+Na]$^+$), 571 ([2M+Na]$^+$); HRMS (FAB): calcd for $C_{14}H_{19}O_2N_4$ ([M+H]$^+$) 275.1508, found 275.1508.

4.1.3. *N*-(7-Methyl-1,8-naphthyridin-2-yl)carbamic acid [1,2-diazenediylbis (4,1-phenylenemethyleneimino-4,1-butanediyl)] ester (4, NCDA4)

To a mixture of **9b** (80 mg, 0.292 mmol) and 4,4′-formylazobenzene **11** (31.6 mg, 0.13 mmol) in $CHCl_3$ (5 mL) and methanol (2.5 mL) was added acetic acid (19.0 mL, 0.33 mmol) and the reaction mixture was stirred at ambient temperature for 1 h. Sodium cyanotrihydroborate ($NaBH_3CN$) (16.7 mg, 0.27 mmol) was added to the reaction mixture. After 2.5 h stirring, solvent was removed in vacuo and the residue was diluted with saturated aqueous $NaHCO_3$ solution and extracted with $CHCl_3$. The organic phase was washed with brine, dried over anhydrous $MgSO_4$, filtered, and concentrated in vacuo. The crude product was purified by column chromatography on silica gel ($CHCl_3$/methanol = 20:1) to give **4** (49.5 mg, 0.066 mmol, 50%) as an orange solid: ^{1}H NMR (400 MHz, $CDCl_3$) δ = 1.60 (m, 4H), 1.73 (m, 4H), 2.65–2.68 (10H), 3.83 (s, 4H), 4.18 (t, 4H, *J* = 6.5 Hz), 7.14 (d, 2H, *J* = 8.3 Hz), 7.40 (d, 4H, *J* = 8.1 Hz), 7.63 (br, 2H), 7.80 (d, 4H, *J* = 8.1 Hz), 7.92 (d, 2H, *J* = 8.3 Hz), 8.04 (d, 2H, *J* = 8.8 Hz), 8.19 (d, 2H, *J* = 8.8 Hz); ^{13}C NMR (150 MHz, $CDCl_3$) δ = 25.95, 26.70, 26.98, 49.17, 53.92, 66.05, 112.93, 118.30, 121.64, 123.24, 129.05, 136.73, 139.29, 143.77, 152.11, 153.55, 153.69, 155.04, 163.54; ESI-MS, *m*/e 777 ([M+Na]$^+$); HRMS (FAB): calcd for $C_{42}H_{47}O_4N_{10}$ ([M+H]$^+$) 755.3782, found 755.3772.

4.1.4. 2-(*tert*-Butyldiphenylsilyloxy)ethylmine (16)

To a solution of 2-aminoethanol **15** (1.06 g, 17.3 mmol) in dry DMF (20 ml) was added *t*-butylchlorodiphenyl silane (4.58 g, 17.3 mmol) and imidazole (1.18 g, 17.4 mmol). The reaction mixture was stirred at ambient temperature for 3 h. Then the solvent was concentrated in vacuo. The residue was diluted with $CHCl_3$, washed with saturated aqueous $NaHCO_3$, H_2O and brine, and dried over anhydrous $MgSO_4$. The solvent was evaporated in vacuo and the crude residue was purified by column chromatography on silica gel ($CHCl_3$/methanol = 25:1) to give **16** (1.30 g, 4.34 mmol, 25%) as a pale-yellow oil: ^{1}H NMR (400 MHz, DMSO) δ 0.98 (s, 9H), 266 (t, 2H, *J* = 6.08 Hz), 3.58 (t, 2H, *J* = 4.88 Hz), 7.43 (m, 6H), 7.61 (m, 4H); ^{13}C NMR (100 MHz, $CDCl_3$) δ 18.9, 26.5, 43.9, 65.8, 127.3, 129.3, 133.3, 135.2; HRMS (ESI) calcd for $C_{18}H_{27}NOSi$ [(M+H)$^+$] 300.1783, found 300.1779.

4.1.5. *N,N′*-Bis[2-(*tert*-butyldiphenylsilyloxy)ethyl]-4,4′-aminomethylazobenzene (17)

To a solution of **16** (398 mg, 1.33 mmol) in $CHCl_3$/methanol = 2:1 (12 ml) was added 4,4′-diformylazobenzene **11** (113 mg, 0.475 mmol) and glacial acetic acid (pH 5). The reaction mixture was stirred at ambient temperature for 1 h under argon. To the reaction mixture was added sodium cyanotrihydroborate ($NaBH_3CN$) (83.5 mg, 1.32 mmol). The reaction mixture was stirred at room temperature for 2 h. The solvent was concentrated in vacuo. The residue was diluted with $CHCl_3$, washed with saturated aqueous $NaHCO_3$, H_2O and brine, and dried over anhydrous $MgSO_4$. The solvent was concentrated in vacuo and the crude residue was purified by column chromatography on silica gel (from $CHCl_3$ 100% to $CHCl_3$/methanol = 50:1) to give **17** (306 mg, 0.38 mmol, 80%) as an orange solid: ^{1}H NMR (400 MHz, $CDCl_3$) δ 1.04 (s, 18H), 2.78 (t, 4H, *J* = 5.1 Hz), 3.81 (t, 4H, *J* = 5.1 Hz), 3.88 (s, 4H), 7.34–7.46 (16H), 7.61–7.66 (8H), 7.87 (d, 4H, *J* = 8.3 Hz); ^{13}C NMR (150 MHz, $CDCl_3$) δ 19.3, 27.0, 50.9, 53.2, 63.1, 123.0, 127.8, 128.8, 129.8, 133.6, 135.6, 143.5, 151.9; HRMS (ESI) calcd for $C_{50}H_{61}N_4O_2Si_2$ [(M+H)$^+$] 805.4333, found 805.4326.

4.1.6. *N,N′*-Bis(*tert*-butoxycarbonyl)-*N,N′*-bis[2-(*tert*-butyldiphenylsilyloxy)ethyl]-4,4′-aminomethylazobenzene (18)

To a solution of **17** (276 mg, 0.34 mmol) in $CHCl_3$ (10 mL) was added di-*tert*-butyl dicarbonate (224 mg, 1.03 mmol). The reaction mixture was stirred at ambient temperature for 3 h under argon and concentrated in vacuo. The residue was extracted with ethyl acetate. The organic phase was washed with saturated aqueous $NaHCO_3$, H_2O and brine, and dried over anhydrous $MgSO_4$. The organic phase was concentrated in vacuo and the crude residue was purified by column chromatography on silica gel ($CHCl_3$/methanol = 200:1) to give **18** (345 mg, 0.343 mmol, quantitative yield) as an orange oil. The NMR spectra showed the rotameric mixture due to high rotation barriers caused by the tertiary amide bond of *t*-Boc protective group: ^{1}H NMR (400 MHz, $CDCl_3$) (rotameric mixture) δ 1.04 (s, 18H), 1.41 (s, 18H), 3.32–3.44 (4H), 3.71–3.80 (4H), 4.57–4.61 (4H), 7.32–7.43 (16H), 7.60–7.64 (8H), 7.84 (d, 4H, *J* = 8.0 Hz); ^{13}C NMR (150 MHz, $CDCl_3$) (rotameric mixture) δ 19.1, 26.8, 28.3, 48.5, 48.8, 50.8, 51.6, 62.4, 62.5, 79.8, 85.1, 122.9, 127.7, 128.2, 129.7, 133.3, 135.5, 141.7, 142.1, 151.8, 155.5, 155.8; HRMS (ESI) calcd for $C_{60}H_{76}N_4O_6Si_2Na$ [(M+Na)$^+$] 1027.5201, found 1027.5172.

4.1.7. *N,N′*-Bis(*tert*-butoxycarbonyl)-*N,N′*-bis(2-hydroxyethyl)-4,4′-aminomethylazobenzene (19)

To a solution of **18** (368 mg, 0.37 mmol) in THF (7.5 mL) was added TBAF (1 M in THF) (1.6 mL, 5.6 mmol) and acetic acid (50 μL, 0.87 mmol) and the mixture was stirred at ambient temperature for 12 h. To the reaction mixture was added additional TBAF (0.2 mL, 0.70 mmol) at ambient temperature. Then the solvent was concentrated in vacuo and the crude product was extracted with ethyl acetate. The organic phase was washed with saturated aqueous $NaHCO_3$, H_2O and brine, and dried over anhydrous $MgSO_4$. The solvent was concentrated in vacuo and the crude residue was purified by column chromatography on silica gel ($CHCl_3$/methanol = 30:1) to give **19** (190 mg, 0.359 mmol, 98%) as an orange oil. The NMR spectra showed the rotameric mixture due to high rotation barriers

caused by the tertiary amide bond of *t*-Boc protective group: ^{1}H NMR (400 MHz, $CDCl_3$) (rotameric mixture) δ 1.44 (s, 18H), 3.43 (4H), 3.58–3.72 (4H), 4.39–4.53 (4H), 7.36 (d, 4H, J = 7.56 Hz), 7.86 (d, 4H, J = 8.32); ^{13}C NMR (150 MHz, $CDCl_3$) (rotameric mixture) δ 28.3, 49.1, 50.1, 50.9, 51.9, 61.3, 62.3, 80.3, 123.1, 127.6, 128.3, 141.4, 151.9, 157.3; HRMS (ESI) calcd for $C_{28}H_{40}N_4O_6Na$ [(M+Na)$^+$] 551.2845, found 551.2846.

4.1.8. *N*-(7-Methyl-1,8-naphthyridin-2-yl)carbamic acid [1,2-diazenediylbis [(4,1-phenylenemethylene)(*tert*-butoxycarbonyl)amino-2,1-ethanediyl]] ester (21)

To a solution of **19** (37 mg, 0.07 mmol) in CH_3CN (2.6 mL) was added *N*,*N*′-dissuccinimidyl carbonate (DSC) (62 mg, 0.24 mmol) and triethylamine (48 μL, 0.33 mmol) and the reaction mixture was stirred at ambient temperature under argon for 3 h. To the reaction mixture was added additional DSC (18 mg, 0.081 mmol) diluted with CH_3CN (0.5 mL). After 2 h stirring, the solvent was concentrated in vacuo and the crude product was extracted with ethyl acetate. The organic layer was washed with saturated aqueous $NaHCO_3$ solution, H_2O and brine, and dried over anhydrous $MgSO_4$. The solvent was concentrated in vacuo and the crude residue was purified by column chromatography on silica gel ($CHCl_3$/methanol = 200:1) to give crude *N*-hydroxysuccinimidyl carobonic ester **20** (45.2 mg). To a solution of **20** (44 mg, 0.054 mmol) in CH_2Cl_2 (2 mL) was added 2-amino-7-methyl-1,8-naphthyridine **12** (30 mg, 0.018 mmol) and triethylamine (34 μL, 0.23 mmol) and the reaction mixture was stirred at ambient temperature for 1 day. Then the solvent was concentrated in vacuo and the crude product was extracted with ethyl acetate. The organic layer was washed with saturated aqueous $NaHCO_3$, H_2O and brine, and dried over anhydrous $MgSO_4$. The solvent was concentrated in vacuo and the crude residue was purified by column chromatography on silica gel (from $CHCl_3$ 100% to $CHCl_3$/methanol = 100:1) to give **21** (34 mg, 0.037 mmol, 56% 2 steps) as an orange solid. The NMR spectra showed the rotameric mixture due to high rotation barriers caused by the tertiary amide bond of *t*-Boc protective group: ^{1}H NMR (400 MHz, $CDCl_3$) (rotameric mixture) δ 1.34−1.50 (18H), 2.72 (s, 6H), 3.50–3.61 (4H), 4.28–4.35 (4H), 4.55–4.59 (4H), 7.20–7.22 (2H), 7.32 (4H), 7.75 (4H), 7.93 (4H), 7.98 (2H), 8.07 (2H), 8.18–8.20 (2H); ^{13}C NMR (150 MHz, $CDCl_3$) (rotameric mixture) δ 25.5, 28.3, 46.1, 46.4, 50.7, 51.7, 63.5, 63.8, 80.5, 112.4, 117.9, 121.3, 127.5, 128.2, 136.3, 139.0, 141.0, 141.3, 151.7, 152.6, 153.0, 154.5, 155.7, 163.2; HRMS (ESI) calcd for $C_{48}H_{54}N_{10}O_8Na$ [(M+Na)$^+$] 921.4023, found 921.4021.

4.1.9. Hydrochloride salt of *N*-(7-methyl-1,8-naphthyridin-2-yl)carbamic acid [1,2-diazenediylbis(4,1-phenylenemethyleneimino-2,1-ethanediyl)] ester (2, NCDA2)

To a solution of **21** (32 mg, 0.036 mmol) in $CHCl_3$ (6 mL) was added ethyl acetate containing 4 M HCl (6 mL) and the reaction mixture was stirred at room temperature for 2.5 h. The solvent was concentrated in vacuo and freeze-dried to give **2** (quantitative yield) as an orange solid: ^{1}H NMR (600 MHz, D_2O) δ 2.73 (s, 9H), 3.53 (br, 4H), 4.38 (br, 4H), 4.40 (s, 4H), 7.31 (d, 2H, J = 8.4), 7.36 (d, 4H, J = 8.1), 7.57 (d, 4H, J = 8.4), 7.88 (d, 2H, J = 8.8), 8.27 (d, 2H, J = 8.7), 8.35 (d, 2H, J = 8.4); ^{13}C NMR (150 MHz, D_2O) δ 20.6, 45.5, 50.8, 61.9, 116.6, 119.8, 122.4, 123.9, 132.4, 134.6, 140.9, 146.3, 147.2, 151.8, 153.1, 156.6, 159.5; HRMS (ESI) calcd for $C_{38}H_{38}N_{10}O_4Na$ [(M+Na)$^+$] 721.2975, found 721.2977.

4.1.10. *N*-(7-Methyl-1,8-naphthyridin-2-yl)-3,3′-[1,2-diazenediylbis(4,1-phenylenemethyleneimino)]dipropanamide (1, NDA)

To a solution of **10** (41 mg, 0.18 mmol) and 4,4′-formylazobenzene **11** (21 mg, 0.090 mmol) in $CHCl_3$/CH_3OH = 2:1 (9 ml) was added acetic acid (pH 5). The reaction mixture was stirred at ambient temperature for 1 h. Then to the reaction mixture was added sodium cyanotrihydroborate (7 mg, 0.11 mmol) and the reaction mixture was stirred at ambient temperature for 6 h. To the reaction mixture was added additional sodium cyanotrihydroborate (7 mg, 0.11 mmol) and the reaction mixture was stirred at ambient temperature 18 h. Then the reaction mixture was extracted from $CHCl_3$, washed with brine, and dried over anhydrous $MgSO_4$. The solvent was concentrated in vacuo and the crude residue was purified by column chromatography on silica gel (CHCl3/MeOH = 5:1), GPC (MeOH) and preparative TLC to give **1** (8.6 mg, 0.013 mmol, 14%). The hydrochloric salt of **1** was used for ^{1}H and ^{13}C NMR measurements: ^{1}H NMR (400 MHz, D_2O) δ 2.68 (s, 6H), 2.93 (t, 4H, J = 6.0), 3.44 (t, 4H, J = 6.0), 4.34 (s, 4H), 7.50 (d, 2H, J = 8.5), 7.57 (s, 8H), 8.20 (d, 2H, J = 9.0), 8.41 (d, 2H, J = 9.4), 8.61 (d, 2H, J = 8.3); ^{13}C NMR (150 MHz, D_2O) δ 20.8, 33.2, 43.1, 51.1, 117.9, 120.6, 123.1, 124.0, 131.8, 135.0, 141.3, 146.6, 147.5, 152.6, 156.4, 160.4, 172.0; HRMS (ESI) calcd for $C_{38}H_{39}N_{10}O_2$ [(M+H)$^+$] 667.3257, found 667.3253.

4.2. Measurements of UV–vis spectra

NCDA (6 μM) derivatives or **NDA** (6 μM) was dissolved in a sodium cacodylate buffer (10 mM, pH 7.0) containing NaCl (100 mM). UV–vis absorption spectra was recorded on BECKMAN COULTER DU®800 spectrometer using 1 cm path length cell at ambient temperature before and after photoirradiation at 360 nm for indicated time period.

4.3. HPLC analysis

A solution (total volume 100 μL) containing **NCDA** (80 μM) derivatives or **NDA** (40 μM) in a sodium cacodylate buffer (10 mM, pH 7.0) containing NaCl (100 mM) was irradiated using an ASAHI SPECTRA LAX-102 equipped with 360 nm band path filter at a distance of 10 cm. After photoirradiation for 5 min, the sample solution was analyzed by reverse-phase HPLC on a GILSON system (805 MANOMETRIC MODULE, 811C DYNAMIC MIXER, 305 PUMP, 306 PUMP, 118 UV–vis DETECTOR, Nacalai tesque COSMOSIL packed column (4.6 × 150 mm)) detected at 260 nm; elution with a solvent mixture of 0.1 M triethylammonium acetate (pH 7.0), 5–25% acetonitrile/20 min, and 25–85%/20–60 min at a flow rate 1.0 mL/min.

4.4. Measurements of melting temperature (T_m) of DNA duplexes

The sample solution were prepared by mixing DNA duplex (4.5 μM) and 18.2 μM **NCDA** or **NDA** in 10 mM sodium cacodylate buffer (pH 7.0), and 100 mM NaCl. Thermal denaturation profiles were recorded on a SHIMADZU UV-2550 UV–vis spectrometer equipped with a SHIMADZU TMSPC-8 temperature controller. The absorbance of the samples were monitored at 260 nm from 2 °C to 80 °C with heating rate of 1 °C/min. The measurements were carried out before and after photoirradiation (360 nm, 5 min). The T_m values were determined as the temperature crossing the melting curve and the median of two straight lines drawn for the single and duplex region in the melting curve.

4.5. CSI-TOF-MS measurements of ligand/DNA complex

Samples were prepared by mixing DNA duplex (20 μM, d(CTA ACG GAA TG)/d(CAT TCG GTT AG)) and **NCDA** or **NDA** (0–60 μM) in 50% methanol in water containing 100 mM ammonium acetate. Mass spectra were obtained with a JEOL AccuTOF JMS-T100 N mass spectrometer in the negative ion mode (orifice 1 voltage = −60 V). Spray temperature was fixed at −10 °C with a sample flow rate of

10 μL/min. Nitrogen gas was used as a desolvation gas as well as a nebulizer.

4.6. Calculation of structures

Molecular modeling simulation was carried out with MacroModel 9.1 with an AMBER* force field. Initial structures were constructed manually from the NMR-structure we determined previously.[9b] Energy minimization was done for the initial structures of the complex with Generalized-Born/Surface-Area (GB/SA) solvation treatment of water. Solvent accessible surface area (ASA) was calculated with a probe molecule of radius of 1.4 Å (water) over van der Waals surface. Solvent accessible surfaces of the ligands in the complex were obtained from the calculation of $ASA_L - (ASA_D + ASA_L - ASA_{DL})/2$, where the solvent accessible surface area of the entire complex, the DNA duplex, and ligand extracted from the complex are represented by ASA_{DL}, ASA_D, and ASA_L, respectively. For conformational search, the Monte Carlo Multiple Minimum (MCMM) search protocol was used to generate an initial family of 2000 conformers of the each ligands. Each conformer was energy-minimized using the AMBER* force field in water.

Acknowledgments

This work was supported by Grant in Aid for Scientific Research (S) (18105006) for K.N. and Grant in Aid for Young Scientists (B) (18710187) for CD from the Japan Society for the Promotion of Science.

References and notes

1. Mayer, G.; Heckel, A. *Angew. Chem., Int. Ed.* **2006**, *45*, 4900.
2. (a) Asanuma, H.; Ito, T.; Yoshida, T.; Liang, X.; Komiyama, M. *Angew. Chem., Int. Ed.* **1999**, *38*, 2393; (b) Asanuma, H.; Liang, X.; Yoshida, T.; Komiyama, M. *ChemBioChem.* **2001**, *2*, 39.
3. Lewis, F. D.; Liu, X. *J. Am. Chem. Soc.* **1999**, *121*, 11928.
4. Hamad-Schifferli, K.; Schwartz, J. J.; Santos, A. T.; Zhang, S. G.; Jacobson, J. M. *Nature* **2002**, *415*, 152.
5. (a) Horsey, I.; Krishnan-Ghosh, Y.; Balasubramanian, S. *Chem. Commun.* **2002**, 1950; (b) Bianké, H.; Häner, R. *ChemBioChem.* **2004**, *5*, 1063; (c) Göritz, M.; Krämer, R. *J. Am. Chem. Soc.* **2005**, *127*, 18016.
6. (a) Höbartner, C.; Mittendorfer, H.; Breuker, K.; Micura, R. *Angew. Chem., Int. Ed.* **2004**, *43*, 3922; (b) Höbartner, C.; Silverman, S. K. *Angew. Chem., Int. Ed.* **2005**, *44*, 7305; (c) Ghosn, B.; Haselton, F. R.; Gee, K. R.; Monroe, W. T. *Photochem. Photobiol.* **2005**, *81*, 953; (d) Heckel, A.; Buff, M. C. R.; Raddatz, M.-S. L.; Müller, J.; Pötzsch, B.; Mayer, G. *Angew. Chem., Int. Ed.* **2006**, *45*, 6748; (e) Tanabe, K.; Kanezaki, H.; Ishii, H.; Nishimoto, S. *Org. Biomol. Chem.* **2007**, *5*, 1242.
7. (a) Ordoukhanian, P.; Taylor, J.-S. *J. Am. Chem. Soc.* **1995**, *117*, 9570; (b) Ando, H.; Furuta, T.; Tsien, R. Y.; Okamoto, H. *Nat. Gen.* **2001**, *28*, 317; (c) Rotaru, A.; Mokhir, A. *Angew. Chem., Int. Ed.* **2007**, *46*, 6180; (d) Tang, X.; Maegawa, S.; Weinberg, E. S.; Dmochowski, I. J. *J. Am. Chem. Soc.* **2007**, *129*, 11000; (e) Shestopalov, I. A.; Sinha, S.; Chen, J. K. *Nat. Chem. Biol.* **2007**, *3*, 650.
8. (a) Peng, T.; Dohno, C.; Nakatani, K. *Angew. Chem., Int. Ed.* **2006**, *45*, 5623; (b) Peng, T.; Dohno, C.; Nakatani, K. *ChemBioChem.* **2007**, *8*, 483.
9. (a) Nakatani, K.; Sando, S.; Saito, I. *Nat. Biotechnol.* **2001**, *19*, 51; (b) Nakatani, K.; Hagihara, S.; Goto, Y.; Kobori, A.; Hagihara, M.; Hayashi, G.; Kyo, M.; Nomura, M.; Mishima, M.; Kojima, C. *Nat. Chem. Biol.* **2005**, *1*, 39; (c) Peng, T.; Nakatani, K. *Angew. Chem., Int. Ed.* **2005**, *44*, 7280.
10. Dohno, C.; Uno, S.; Nakatani, K. *J. Am. Chem. Soc.* **2007**, *129*, 11898.
11. Photoswitchable DNA-binder using photochromic spiropyran has been reported recently: Andersson, J.; Li, S.; Lincoln, P.; Andréasson, J. *J. Am. Chem. Soc.* **2008**, *130*, 11836.
12. Peng, T.; Murase, T.; Goto, Y.; Kobori, A.; Nakatani, K. *Bioorg. Med. Chem. Lett.* **2005**, *15*, 259.
13. Knoll, H. In *CRC Handbook of Organic Photochemistry and Photobiology*; Horspool, W. M., Lenci, F., Eds., 2nd ed.; CRC Press LLC: Boca Raton, FL, 2004; pp 89/1–89/16.
14. Liang, X.; Asanuma, H.; Kashida, H.; Takasu, A.; Sakamoto, T.; Kawai, G.; Komiyama, M. *J. Am. Chem. Soc.* **2003**, *125*, 16408.
15. (a) Griffey, R. H.; Hofstadler, S. A. *Chem. Rev.* **2001**, *101*, 377; (b) Yamaguchi, K. *J. Mass Spectrom.* **2003**, *38*, 473.